The 9th European Congress on Computational Methods in Applied Sciences and Engineering
ECCOMAS Congress 2024
3 – 7 June 2024, Lisboa, Portugal

STUDY OF HEMODYNAMIC IN THE ILIAC BIFURCATION THROUGH FLUID-STRUCTURE INTERACTION SIMULATIONS

FILIPA CARNEIRO[1*], LOURENÇO BASTOS[1], SENHORINHA TEIXEIRA[2] AND JOSÉ CARLOS TEIXEIRA[3]

[1] PIEP - Innovation in Polymer Engineering
University of Minho, Campus of Azurém, Edificio 15,
4800-058, Guimarães, Portugal
e-mail: f.carneiro@piep.pt , www.piep.pt

[2] University of Minho, Department of Production and Systems Engineering,
Campus of Azurém, 4800-058 Guimarães, Portugal

[3] University of Minho, Department of Mechanical Engineering,
Campus of Azurém, 4800-058 Guimarães, Portugal

Key words: Atherosclerosis, cardiovascular modelling, fluid structure interaction

Summary

The FSI numerical studies allowed the velocity distribution analysis along the geometric domain. A recirculation bubble is formed in each of the two iliac arteries, immediately downstream the iliac bifurcation, being consequently, a region prone to plaque deposition. Atherosclerosis is essentially developed during the deceleration phase of the cardiac cycle, due to the high oscillation of the wall shear stress that increases the size and duration of the recirculation bubble. Unbalanced flow distribution in the iliac arteries enhances the likelihood of flow separation in the starved branch of the cardiovascular system. It was concluded that the wall compliance plays a very important role in the development of disease and should not be neglected. The parameters that may affect the disease are the iliac bifurcation geometry, wall compliance and different distributions of the outflow by the two iliac arteries, probably due to stenosis in the subsequent arteries.

1 INTRODUCTION

Cardiovascular diseases are the leading cause of death in Europe and in the United States of America. One of the most common cardiovascular diseases is atherosclerosis, which is characterized by the presence of deposits in intimal wall of small and medium arteries, including fat substances, calcium, elements and other products transformed of blood flow [1]. This set of deposits is called plaque originating a kind of arterial wall thickness. Plaque development occurs more often at complex flow zones, where the artery is bifurcated, curved and has a junction. The objective of this research is to quantify the relationship between atherogenesis and features in hemodynamics when a flexible artery is assumed. The effect of different wall compliance was studied in a realistic bifurcated segment of an iliac artery.

The numerical research was carried out using Ansys workbench: Fluent for the Computational Fluid Dynamic (CFD) and Ansys Mechanical for structural analysis. It will be considered pulsatile blood flow within a realistic bifurcated segment of iliac artery, able to reproduce the infra-renal cardiac cycle, particular of the abdominal aorta downstream the renal arteries. The pulsatile profile of this cycle presents the specificity of including a period of reverse flow, or a backflow. Blood flow is turbulent and well predicted by the incompressible form of the Navier-Stokes equations.

The elasticity or stiffness of blood vessels has great importance, since it directly influences the way that blood flows inside veins and arteries. Some studies were found in the literature that analyze the elastic properties of veins and arteries [2–10], inclusively for different veins and arteries and for different flow conditions, such as different levels of strain rate [9] and pressure [3]. Also, important to note, as mentioned by Wuyts et al. [8], the stress-strain relationships of blood vessels are strongly nonlinear which makes it impossible to define a single Young's modulus describing the stiffness of an entire blood vessel. In order to cope with this problem, many authors have used an incremental modulus as introduced by Bergel [10]. This modulus represents the slope of the pressure-radius curve at a given level of pressure.

The study presented by Wuyts et al. [8] is particularly interesting, since it presents the analysis of the influence of age and degree of atherosclerosis on the mechanical properties of blood vessels, showing a significant increase in stiffness due to both these factors.

Some works [11-15] have used a numerical FSI (Fluid-Structure Interaction) methodology to analyze the influence of artery elasticity on the blood flow in the iliac bifurcation or in liliac bifurcation in an abdominal aortic aneurysm. Interesting examples are the works of Luo et al. [11] and Kotmakova et al. [12], which are similar to the work here developed. In both these works, an FSI approach is used to evaluate the influence of artery elasticity on the blood flow in the iliac bifurcation. However, these works consider a one-way data transfer approach for this purpose, while a two-way approach is considered in the work presented here.

Previously, Carvalho et al. [1] analyzed the blood flow for a rigid anatomical model of an iliac bifurcation. This work analyses the effect of different material properties of the veins, in hemodynamics and consequently disease development.

2 MATERIALS AND METHODS

In this study, a numerical approach was used to analyze the influence of the vein/artery elasticity on the blood flow, representing different levels of disease on the iliac bifurcation. As previously mentioned, following the work of Carvalho et al. [1], where the blood flow is analyzed for an anatomical model of an iliac bifurcation, in this work the influence of the elasticity of this artery on the blood flow, representing different levels of disease.

2.1 Mathematical equations / Computational model

The numerical simulations were performed were performed using the Fluid-Structure Interaction (FSI) technology from the Ansys software suite (Ansys, Inc., Canonsburg, PA, USA), implemented as a two-way FSI data transfer. In this approach, the CFD (Computational Fluid Dynamics) simulations are performed in the software Fluent® and the structural simulations, which analyze the artery wall behavior, are performed in the software

Mechanical®, in a structural transient simulation. Data transfer between these two solvers is managed by the Ansys System Coupling module.

The CFD numerical simulations were performed considering the k-ε Turbulent Model with Enhanced Wall Treatment algorithm and a conversion criterion of 1E-5. The software Fluent solves the three-dimensional equations for mass, Equation (1) and momentum, Equation (2) assuming conservation for each variable:

$$\nabla \vec{v} = 0 \tag{1}$$

$$\frac{\partial}{\partial t}(\rho \vec{v}) + \nabla(\rho \vec{v}\vec{v}) = \nabla p + \nabla(\bar{\bar{\tau}}) \tag{2}$$

Where $\vec{v}$ is the fluid velocity vector, ρ is the density, p is the static pressure, $\bar{\bar{\tau}}$ is the stress tensor, k_{eff} is the effective conductivity, and S_h other heat sources. The turbulence model is described by Equations (4) and (5):

$$\frac{\partial}{\partial t}(\rho k) + \nabla(\rho \vec{v} k) = \nabla\left[\left(\mu + \frac{\mu_t}{\sigma_k}\right)\frac{\partial k}{\partial x_j}\right] + G_k - \rho\varepsilon\,, \qquad \mu_t = \rho C_\mu \frac{k^2}{\varepsilon} \tag{3}$$

$$\frac{\partial}{\partial t}(\rho \varepsilon) + \nabla(\rho \vec{v} \varepsilon) = \nabla\left[\left(\mu + \frac{\mu_t}{\sigma_\varepsilon}\right)\frac{\partial \varepsilon}{\partial x_j}\right] + C_{1\varepsilon}\frac{\varepsilon}{k}G_k - C_{2\varepsilon}\rho\frac{\varepsilon^2}{k} \tag{4}$$

where k is the kinetic energy, ε the dissipation rate, μ the viscosity, and μ_t the turbulent (or eddy) viscosity. G_k represents the generation of turbulence kinetic energy due to the mean velocity gradients. $C_{1\varepsilon}$, $C_{2\varepsilon}$ and C_μ are constants, 1.44, 1.92 and 0.09, respectively. σ_k = 1.0 and σ_ε = 1.3 are the turbulent Prandtl numbers for k and ε, respectively.

Regarding the mechanical numerical simulations, the software Mechanical solves the general equation of motion, Equation (5), for transient dynamic analyses:

$$\{F(t)\} = M\{\ddot{u}\} + C\{\dot{u}\} + K\{u\} \tag{5}$$

Where F is the load vector at each time instant, t, M is mass matrix, C the damping matrix, K the stiffness matrix, {ü} the nodal acceleration vector, $\{\dot{u}\}$ the nodal velocity vector and {u} the nodal displacement vector.

2.2 Geometrical model

In this work, a realistic model of an iliac bifurcation was considered. This model was constructed by Carvalho et al. [1] through the analysis of real anatomic data, obtained in a DICOM (Digital Imaging and Communications in Medicine) format, and processed using the MIMICS software, from Materialise. The realistic model obtained is shown in Figure 1. The processed model was then simplified into the geometry used in the numerical simulations, since the 3D model obtained directly from rendering the CT images had too many interferences in its surfaces.

For the FSI (Fluid-Structure Interaction) model, more specifically for the structural part of the simulation, a shell surface with a thickness of 1 mm was considered to represent the artery wall. A thickness of 2 mm was also analyzed, since the wall thickness of the iliac bifurcation should be between 1 and 2 mm.

2.3 Geometrical domain discretization

For the fluid domain, a global element size of 1 mm was considered for the domain discretization, or mesh creation. Moreover, 5 boundary layers, with a first layer thickness of 0.3 mm and a growth rate of 1.2, were considered at the cross-section throughout the entire fluid domain. Considering these parameters, the fluid domain was divided into 264,059 tetrahedral elements.

Regarding the structural model, a global element size of 0.75 mm was considered for the mesh creation, with a refinement to 0.5 mm in the bifurcation area. Following these parameters, the shell surface was divided into 6552 triangular and square elements.

The meshes created for both the fluid and structural domains are presented in Figure 2.

a) b)

Figure 1: a) Detailed rendering of the iliac bifurcation; b) Simplified model of the iliac bifurcation used in the simulations.

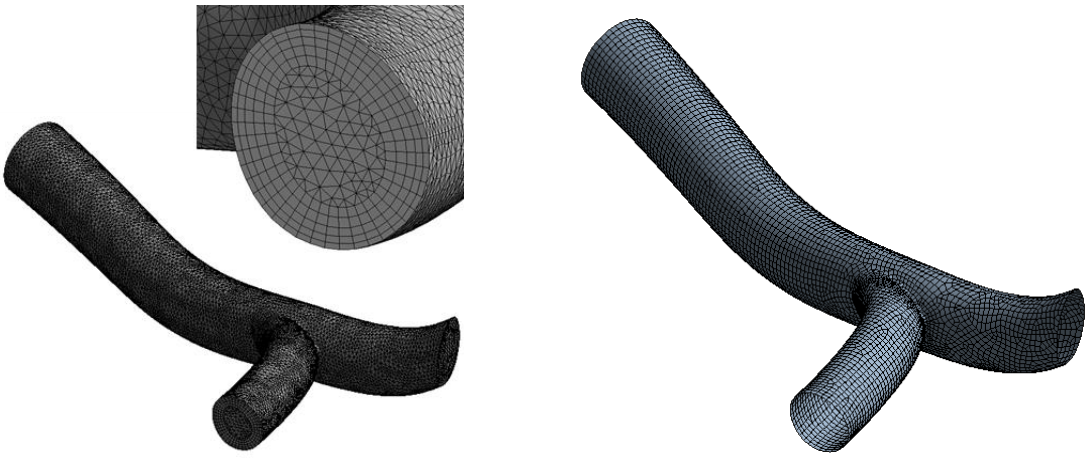

a) b)

Figure 2: Meshes created for a) The fluid domain; b) The artery wall.

2.4 Materials

Regarding the flow properties, the same assumptions considered by Carvalho et al. [1] were implemented, i.e., the numerical simulations were carried out considering a Newtonian and incompressible fluid, for which a viscosity of 0.0004 kg/m.s and a density of 1057 kg/m^3 were assumed for the blood flow.

Concerning the wall of the iliac bifurcation, a linear elastic model was considered to model its mechanical/structural behavior. To analyze different levels of disease on the iliac bifurcation, typical elasticity moduli were analyzed, more specifically 2 MPa, 4 MPa and 8MPa, and a Poisson ratio of 0.4 was considered.

2.5 Boundary conditions

The applied boundary conditions were based in the work developed by Carneiro et al. [18], where the inlet velocity profile, as a function of time for the complete cardiac, was approximated to a sinusoidal function through a numerical method. Thus, the same unsteady inlet velocity profile (Figure 3) was applied, representing the pulsatile inlet velocity represented by Equation (6), where the velocity, in m/s, is obtained by multiplying the resulting value by 10^{-2}.

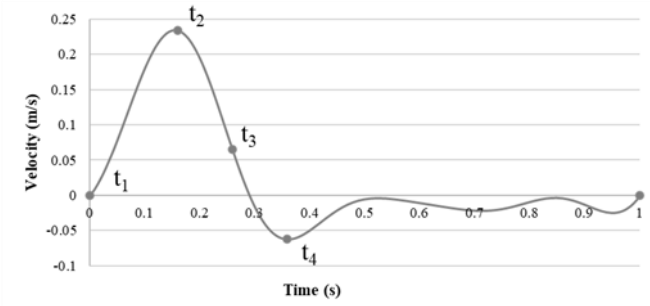

Figure 3: Axial velocity on the inlet with the representation of different time instants: t_1 = 0 s; t_2 = 0.16 s; t_3 = 0.26 s; t4 = 0.36 s. Based on the work of Carneiro et al. [18].

$$\begin{aligned} v(t) = {} & 2.46 + 5.10\cos(2p\,t) - 1.93\cos(4p\,t) - 4.93\cos(6p\,t) \\ & -0.919\cos(8p\,t) + 5.81\sin(2p\,t) + 6.72\sin(4p\,t) \\ & +0.395\sin(6p\,t) - 1.07\sin(8p\,t) \end{aligned} \quad (6)$$

Furthermore, regarding the structural simulations, the inlet and outlet surfaces were considered to be rigidly fixed, and through the data transferred via the Ansys System Coupling module, the pressure on the wall, applied by the blood flow, is transferred from the flow simulations (Fluent) to the structural simulation (Mechanical).

3 RESULTS AND DISCUSSION

3.1 Artery displacement and stress

Results were analyzed for the main time instants represented in Figure 3, namely t_1 = 0 s, t_2 = 0.16 s, t_3 = 0.26 s and t_4 = 0.36 s.

Starting with the results obtained through the structural simulations, total deformations and stresses were analyzed. Figure 4 a), Figure 5 a) and Figure 6 a) show the results obtained for the most relevant time instants, namely t_2 = 0.16 s, t_3 = 0.26 s and t_4 = 0.36 s, respectively. Moreover, in Figure 4 b), Figure 5 b) and Figure 6 b) the total deformations observed are again shown with 10x scale, in order to facilitate the observation of the behavior of the artery.

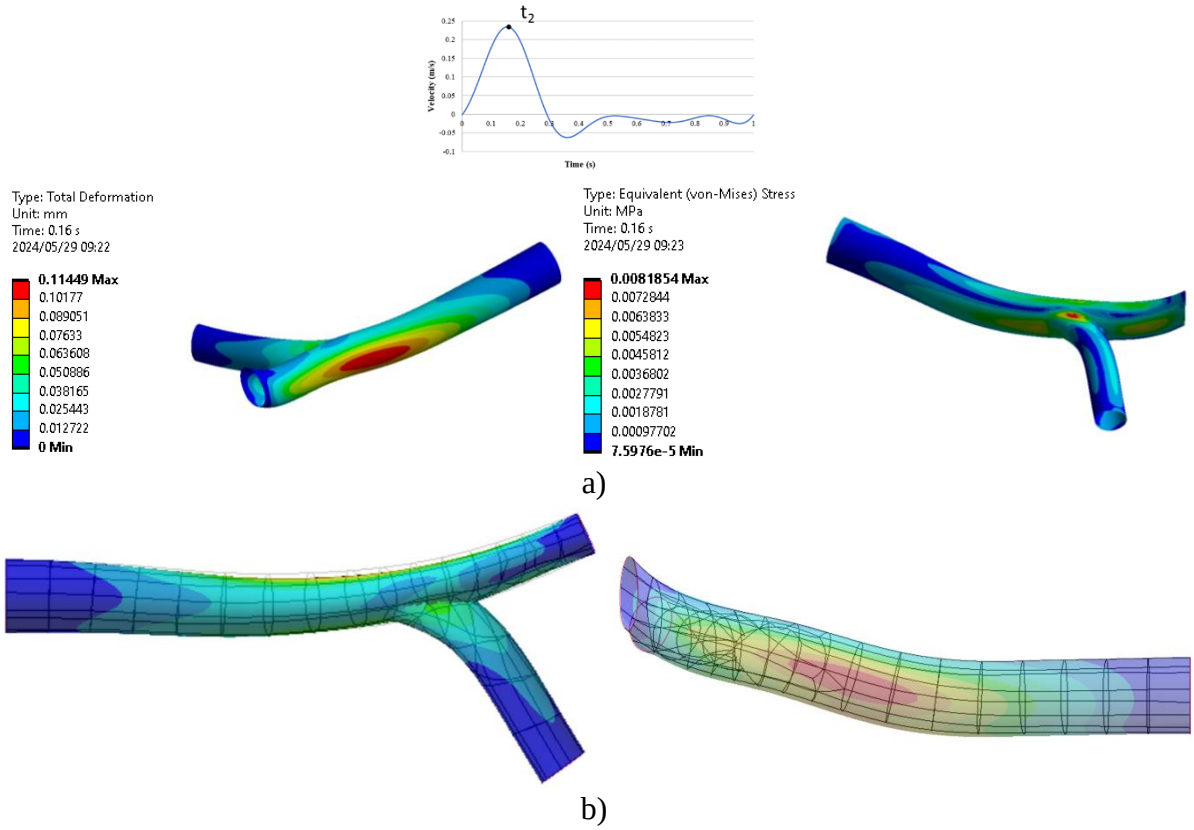

Figure 4: a) Deformation and stress results obtained at t2 = 0.16 s; b) Deformation obtained at t_2 with a 10x scale.

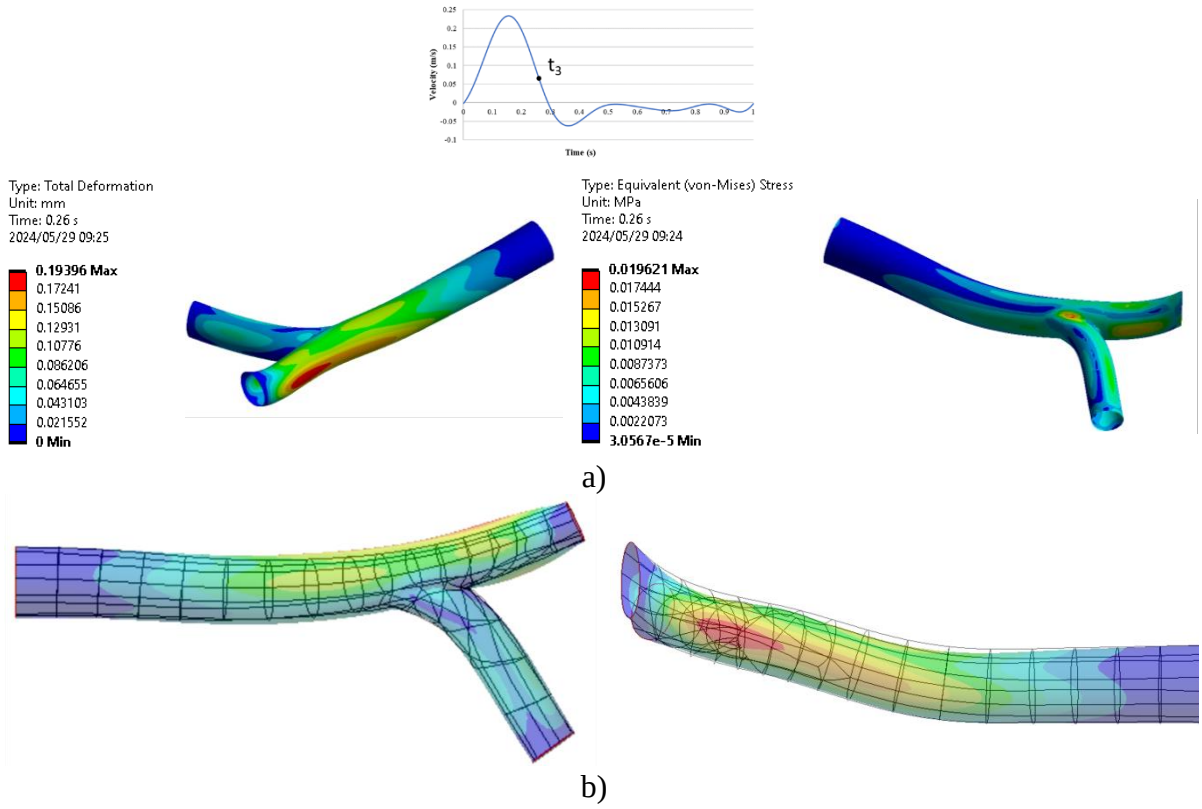

Figure 5: Deformation and stress results obtained for t_3 = 0.26 s; b) Deformation obtained at t_3 with a 10x scale.

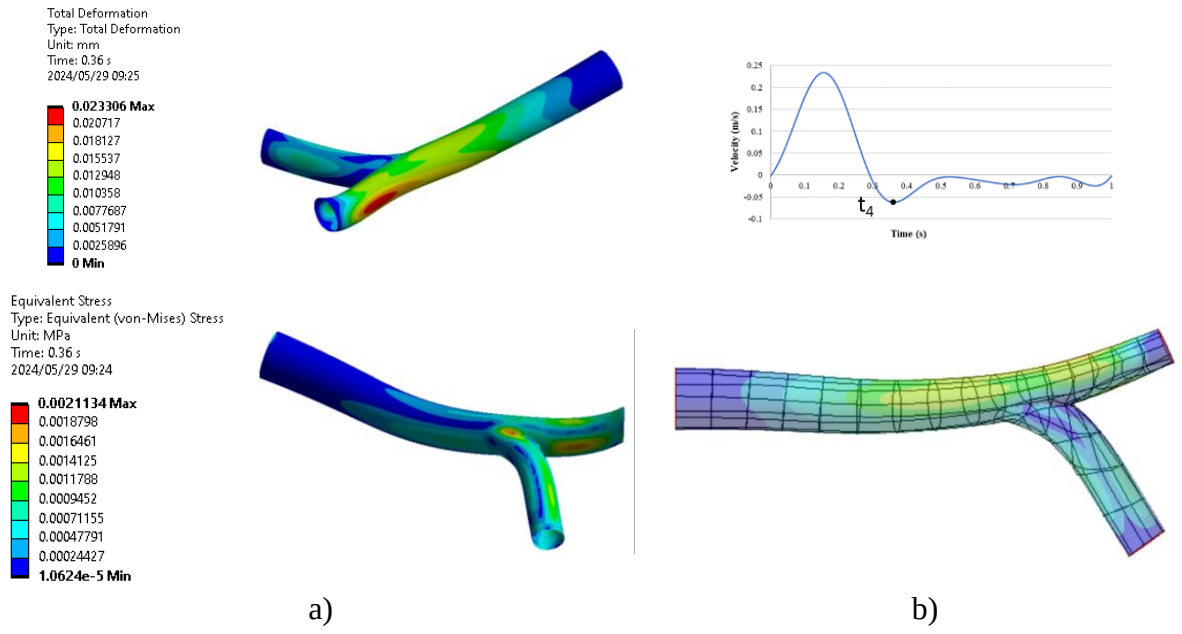

Figure 6: Deformation and stress results obtained for t_4 = 0.36 s; b) Deformation obtained at t_4 with a 10x scale.

As can be observed, for the time instant of 0.36 s no significant deformations are observed, when compared to the other analyzed time instants, being observed a maximum deformation of

0.023 mm and a maximum stress on the artery of 0.0021 MPa. Higher deformations and stresses are observed for 0.16 s, with a maximum deformation of 0.1145 mm and a maximum stress of 0.0082 MPa. As expected, the highest deformations and stresses are observed for 0.26 s, since it corresponds to the time instant with the highest blood pressure. Here, a maximum deformation of 0.194 mm and a maximum stress of 0.0196 MPa are observed, which is considerably higher than the ones observed for other time instants.

Moreover, different behaviors are observed for 0.16 s and 0.26 s, as can also be observed in Figure 4 b) and Figure 5 b). At 0.16 s the artery seems to stretch "vertically" and at 0.26 s the artery seems to stretch "horizontally". This way, at 0.16 s the bifurcation area seems to contract and at 0.26 s it seems to expand, as shown in Figure 7.

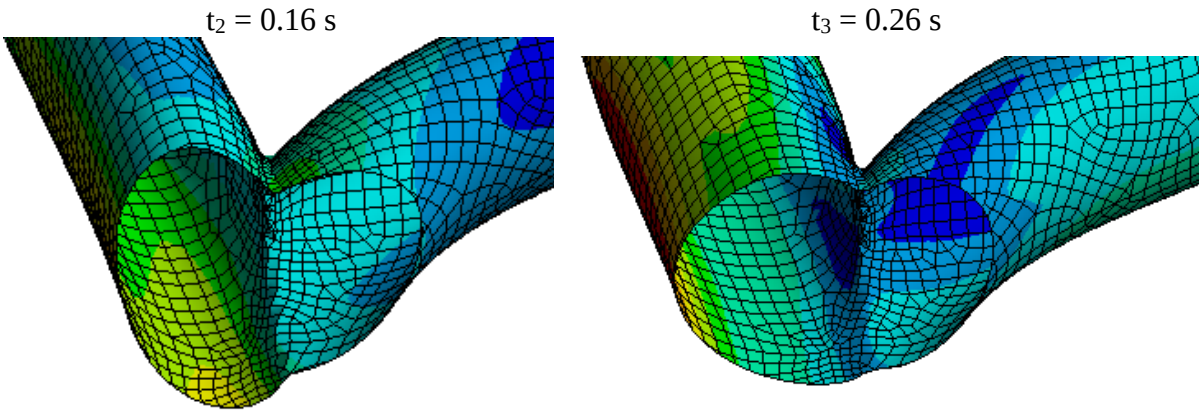

Figure 7: Artery deformation in the bifurcation area (with 10x scale).

In Figure 8, the maximum deformations and stresses, obtained for all the elasticity modulus that were analyzed, are presented.

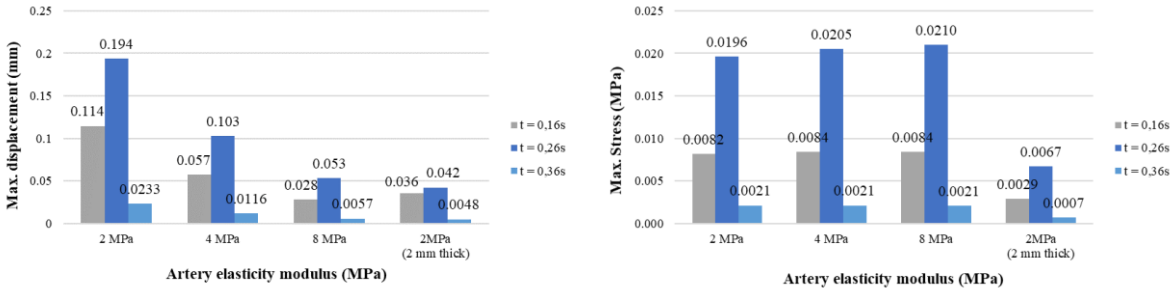

Figure 8: Maximum deformations and stresses observed for all elasticity moduli analyzed.

As can be observed and as expected, an increase in the artery elasticity modulus promotes a decrease in the deformation observed and a slight increase in the maximum stresses. An increase on artery thickness also promotes a considerable decrease in both the maximum deformation and stresses.

3.2 Flow velocity

The vectors of velocity magnitude are presented in Figure 9, for a cut plane going through the bifurcation. Furthermore, the velocity profiles for cross-sections, S1–S9, of the abdominal

aorta, right and left iliac arteries, for the time instants analyzed are presented in Figure 10, Figure 11 and Figure 12, respectively. The cross-sections are outlined in their respective figures. Note that the colored scales were adjusted to allow the assessment of the velocity differences for each location, at different instants of the cardiac cycle. Moreover, velocity magnitude was also analyzed throughout the position (X axis) on the iliac bifurcation, as shown in Figure 13.

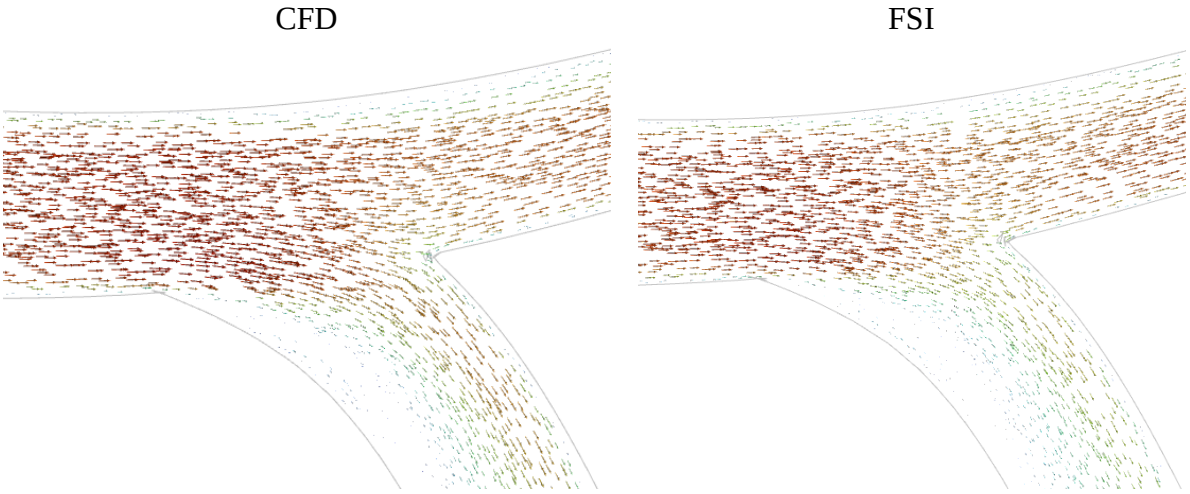

Figure 9: Vector distribution of velocity magnitude at t2 = 0.16 s.

As can be observed, the same flow behavior is observed for the CFD (rigid artery) simulation and the FSI (deformable artery). A slight velocity magnitude decrease is also observed when a deformable artery is used, which was expected due to the artery expansion, although for t = 0.16 s a contraction of the artery is observed in the bifurcation vicinity, which seems to lead to a slight increase in velocity.

The division of flow between the two iliac arteries and the formation of a vortex recirculation in the outer wall of each iliac artery are visible for both the CFD and FSI models, with no major differences noticed between the two models.

To better analyze the differences in velocity magnitude, Figure 13 shows the velocity distribution thorough the X axis, or the length of the iliac bifurcation., for the different time instants analyzed.

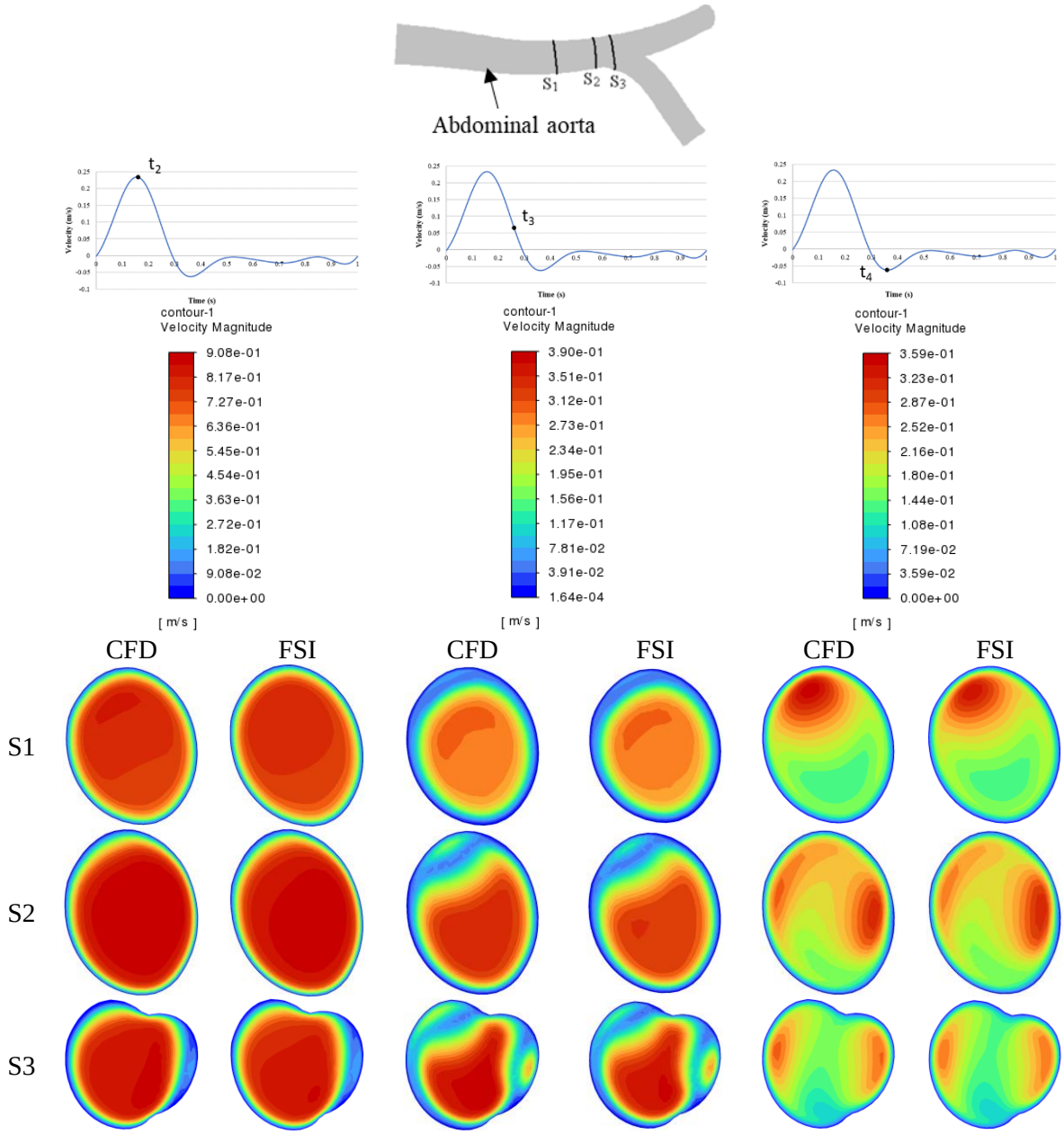

Figure 10: Velocity magnitude (m/s) for different cross-sections during the cardiac cycle at the abdominal aorta.

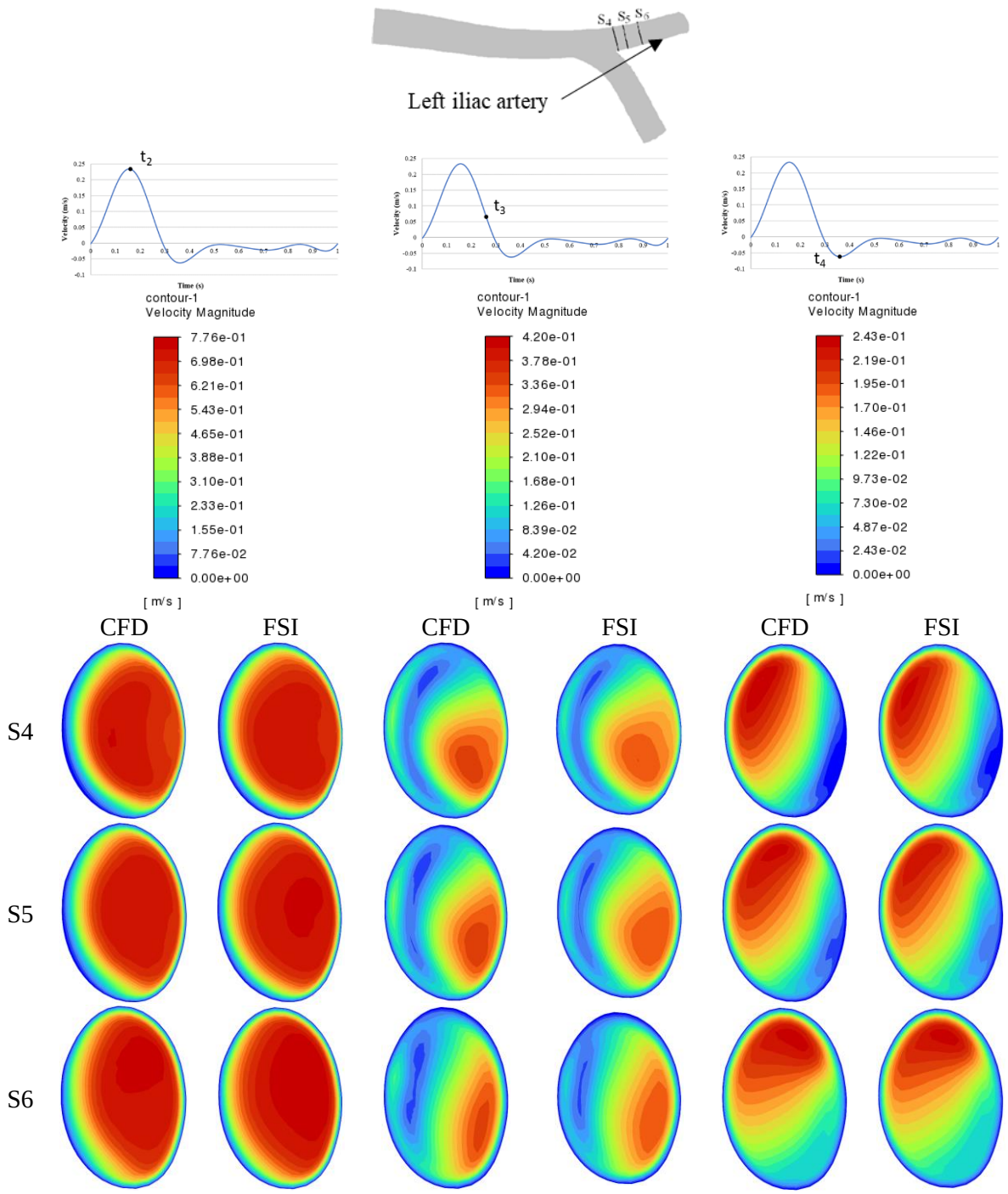

Figure 11: Velocity magnitude (m/s) for different cross-sections during the cardiac cycle at the left iliac artery.

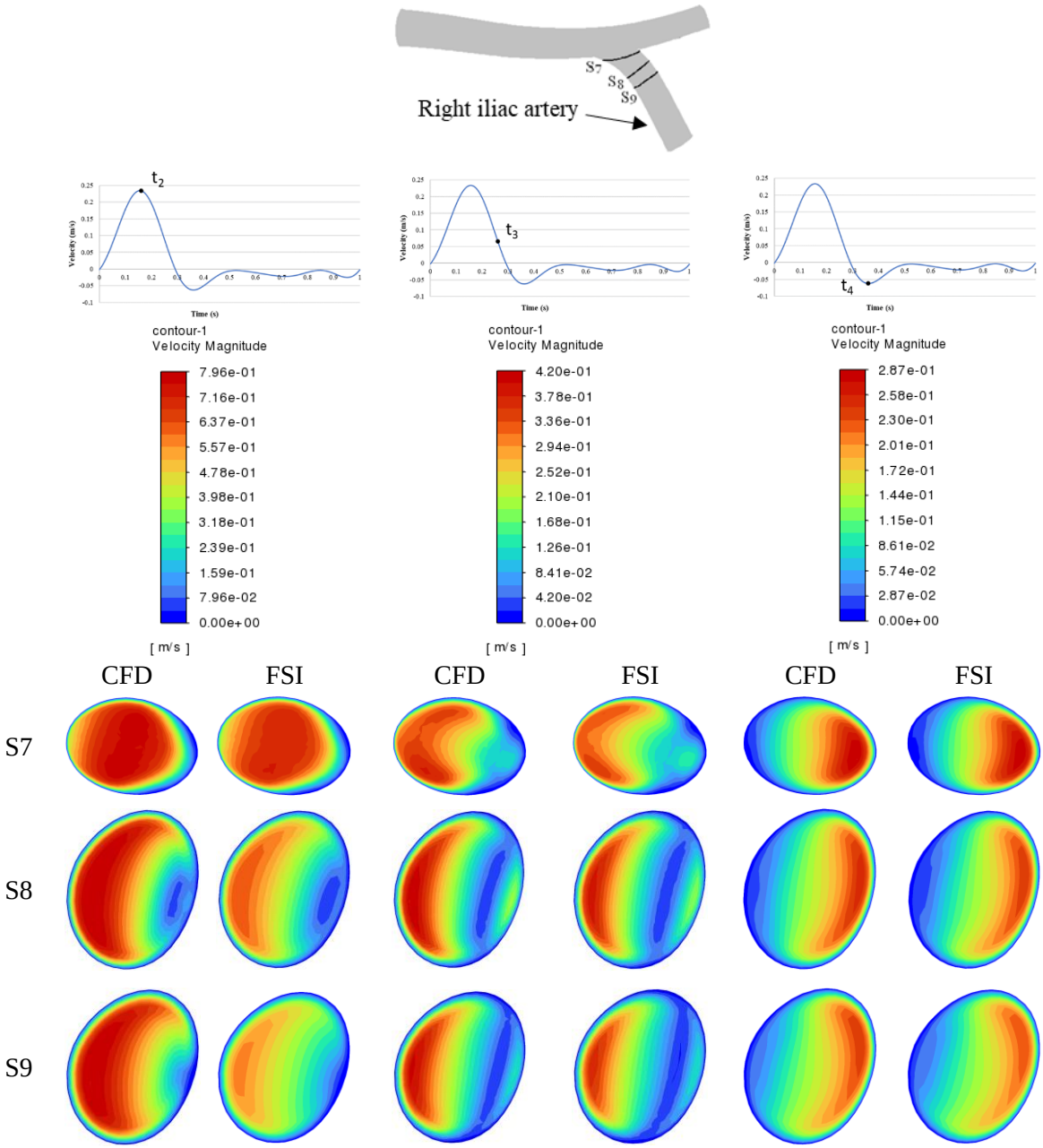

Figure 12: Velocity magnitude (m/s) for different cross-sections during the cardiac cycle at the right iliac artery.

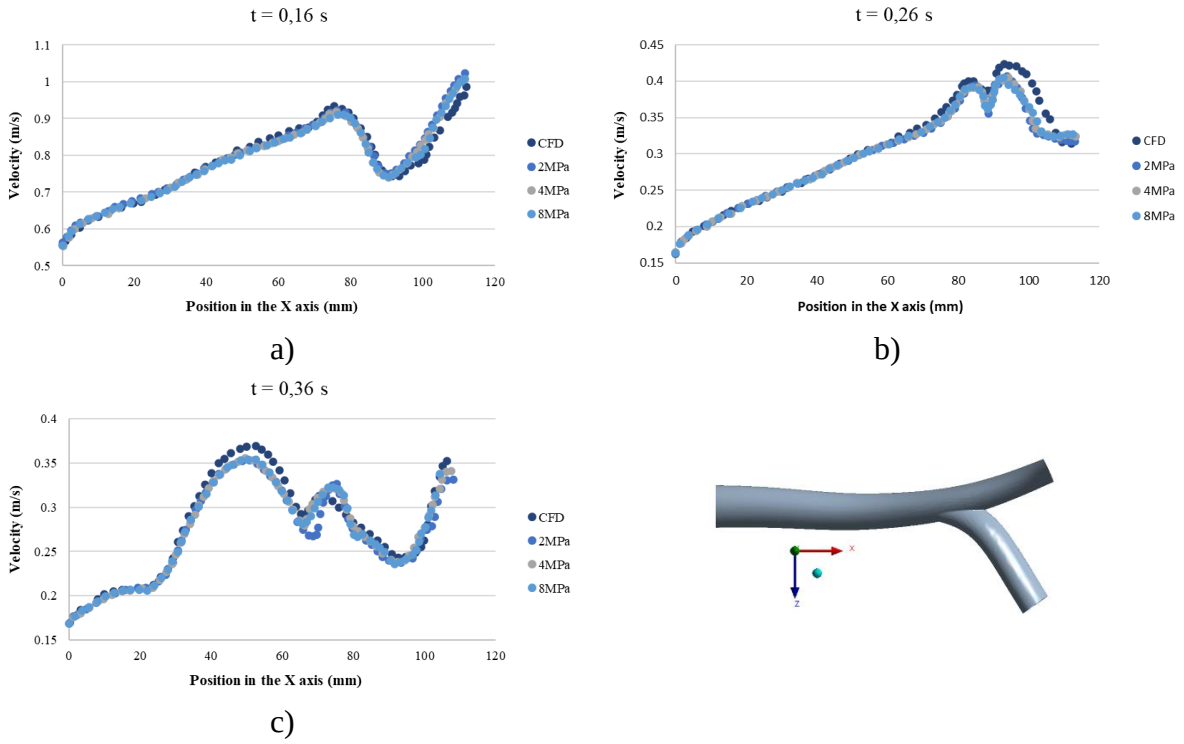

Figure 13: Velocity magnitude distribution throughout the positions in the X axis: a) t_2 = 0.16 s; b) t_3 = 0.26 s; c) t_4 = 0.36 s.

For the first presented time instant, t_2 = 0.16 s, a very slight decrease in velocity is observed for the FSI, similarly to what was observed previously, at least for the abdominal aorta. Contrarily, downward the bifurcation, a slight increase in velocity is observed for the FSI model, more noticeable near the outlet of the left iliac artery (Figure 14). This should be connected to the fact that the bifurcation seems to contract in this time instant, which might justify this increase in velocity downward the bifurcation. Nonetheless, this is just a slight difference, with a maximum velocity magnitude of 0.9857 m/s for the CFD model and of 1.008 m/s for the FSI.

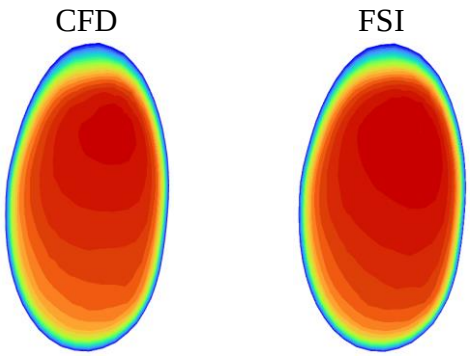

Figure 14: Velocity magnitude at the outlet of the left iliac artery for t_2 = 0.16 s.

For the remaining time steps (t_3 = 0.26 s and t_4 = 0.36s), a slight decrease in velocity is observed, especially after the bifurcation, being more noticeable for t_3, which may be due to the cross-sectional area increase. Again, these are slight differences, which reveals that the CFD model gives similar flow results and that artery elasticity, although important, does not affect considerably the flow behavior inside the artery.

Figure 15 shows the maximum and mass weighted average velocities obtained for the different artery elasticity modulus analyzed, in the 3 time instants mentioned before.

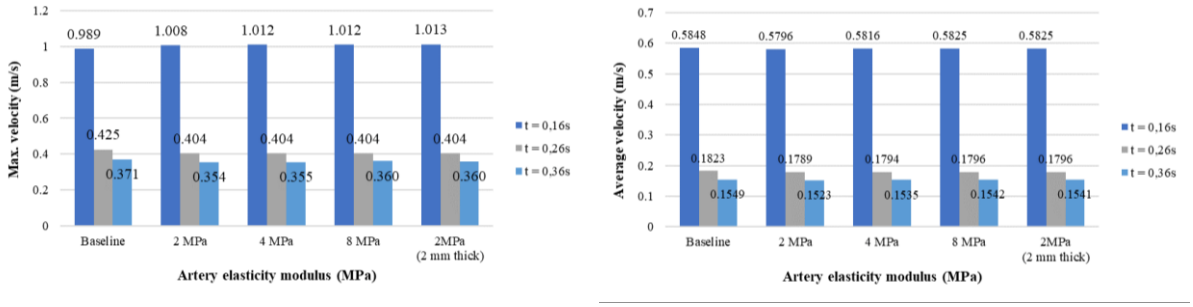

Figure 15: Maximum velocity observed for all elasticity moduli analyzed.

Similarly, to what was observed previously, changing from a CFD to a FSI model promotes a slight increase in the maximum velocity observed but a slight decrease on the average velocity throughout the whole iliac bifurcation. Meaning that, as expected, on average the velocity decreases when a deformable artery is considered, but this also promotes the increase in velocity in certain localized areas. This happens in the time instant t2 = 0.16 s, where the bifurcation seems more contracted, and the highest velocity magnitude is obtained.

Moreover, an increase in the artery elasticity modulus seems to promote a minor increase in both the maximum and the average velocities observed.

3.1 Wall Shear Stress (WSS)

To analyze the differences in WSS between CFD and FSI models, Figure 16 shows the WSS distribution through the X axis, or the length of the iliac bifurcation, for the different time instants analyzed.

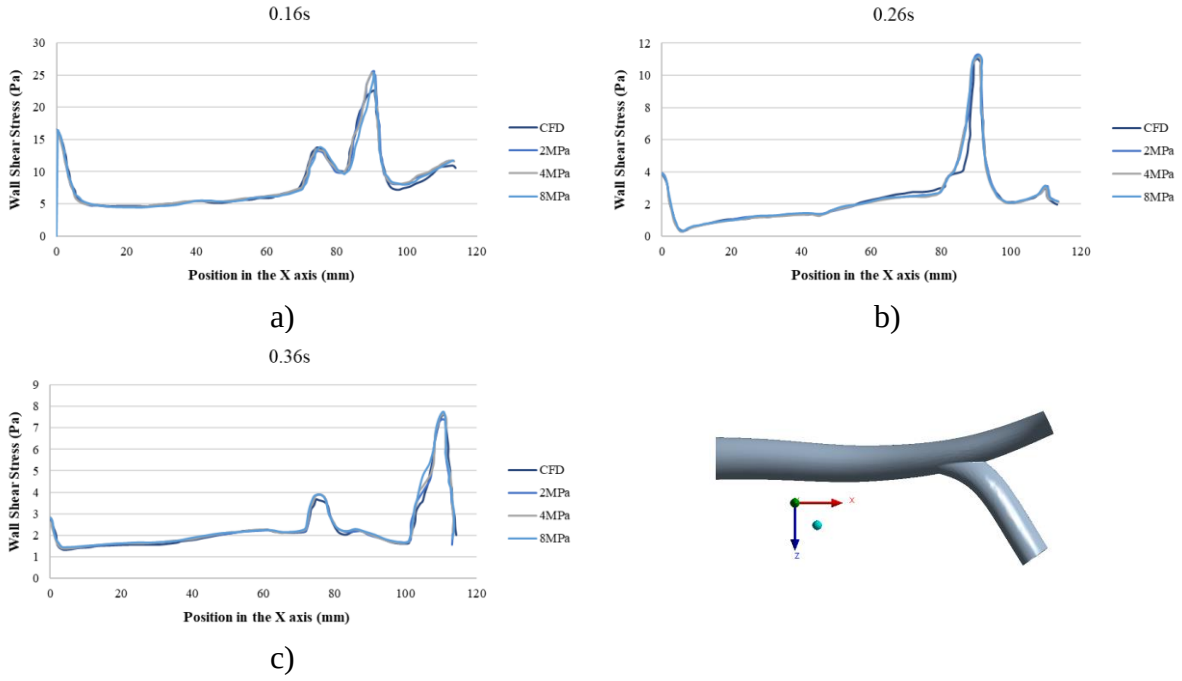

Figure 16: WSS distribution throughout the positions in the X axis: a) t_2 = 0.16 s; b) t_3 = 0.26 s; c) t_4 = 0.36 s.

As can be seen and as expected, the highest WSS (FSI - 25.450 Pa; CFD – 22.515 Pa) is observed for the pulsatile maximum flow peak (t_2 = 0.16 s), where the highest velocity magnitude was also observed. Moreover, for t_2 = 0.16 s and t_3 = 0.26 s the highest WSS is observed in the bifurcation vicinity (Figure 17), while for t_4 = 0.36 s the maximum WSS is observed near the outlet of the left iliac artery. In this time instant, a WSS peak is also observed at the bifurcation vicinity, but with lower value in comparison to the peak near the outlet. This supports the conclusions of Luo et al. [11], stating that the values of WSS are directly affected by the deformation of iliac bifurcation and velocity values.

Similarly to the velocity results, the impact of using a deformable artery is more considerable in the bifurcation vicinity and downstream, due to the artery deformation. On the abdominal aorta no considerable changes are observed.

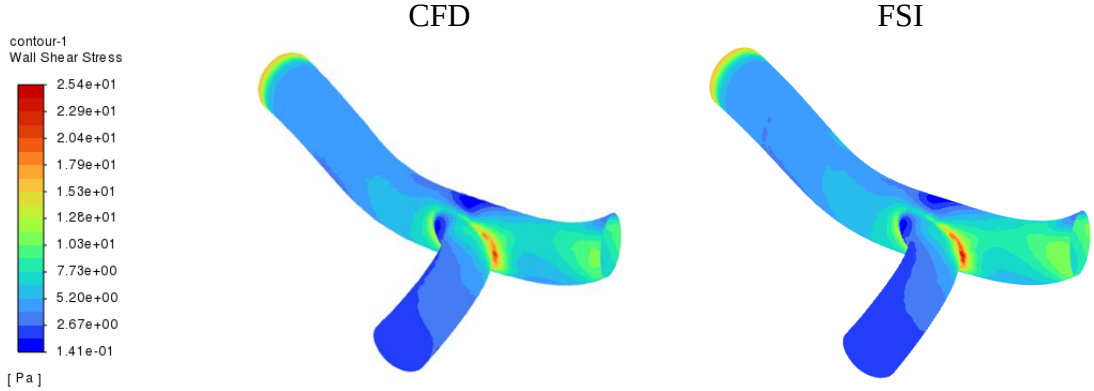

Figure 17: Wall Shear Stress distribution for t*2* = 0.16 s.

The WSS distribution along the geometry is shown in Figure 17. Along the abdominal aorta, the WSS value increases continuously, as can also be observed in Figure 16, reaching the maximum in the bifurcation vicinity. In the outer wall of the iliac artery, the decrease in WSS, reaching really low values, suggests the presence of a recirculation zone close to the wall, which is consistent with the recirculation locations that can be identified in Figure 9 and coincides with a location prone to plaque appearance Moore et al. [16], Lee and Chen [17]. Figure 18 shows the maximum and area weighted average wall shear stress obtained for the different artery elasticity modulus analyzed, in the 3 analyzed time instants.

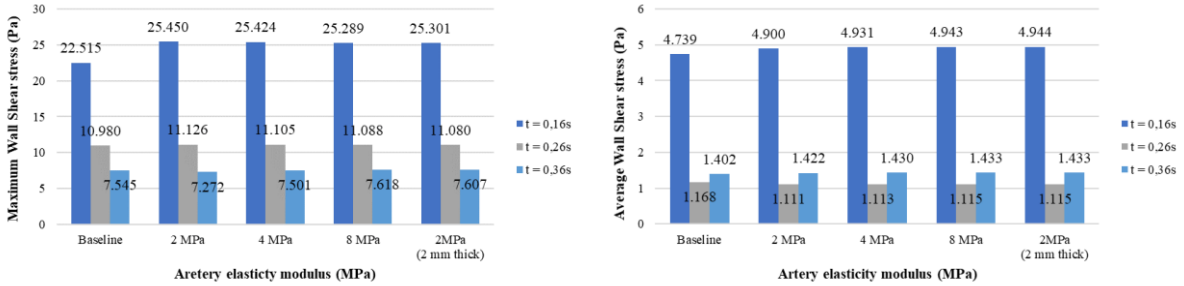

Figure 18: Maximum and average WSS observed for all elasticity moduli analyzed.

As can be observed and as mentioned previously, changing from a CFD to a FSI model promotes an increase in the maximum WSS observed and a slight increase on the average WSS throughout the whole iliac bifurcation. This increase is more noticeable at the time instant t_2, which should be expected, since for this time instant more contraction is observed in the bifurcation and the maximum velocity is obtained. At t_3, even with what seems as an expansion of the artery, which in theory should promote a decrease in WSS, a slight increase in WSS is observed. Thus, it seems that the artery deformation observed is still causing an increase in WSS even with a decrease in the maximum velocity observed at this time instant.

4 CONCLUSIONS

An FSI numerical model based on an anatomical geometry, previously studied by Carvalho et al. [1], was implemented in order to analyze the influence of artery elasticity on the flow dynamics in the bifurcation, namely the abdominal aorta and iliac arteries. This model was then compared with rigid-wall solution (CFD model) of the same anatomical geometry in terms of wall shear stress, flow dynamics (velocity distribution) and artery deformation.

Regarding the artery deformation and stress, the greatest influence in considering artery elasticity is observed in the bifurcation vicinity, where the largest deformations are observed, with a maximum deformation of 0.194 mm. These deformations alter the shape of the bifurcation cross section, varying with the pulsatile velocity considered in the inlet, making the bifurcation contract and expand at different time instants and altering the flow velocity accordingly.

The flow inside the iliac bifurcation did not seem to be majorly affected by considering a deformable artery wall. Although deformations were noticed, especially in the bifurcation vicinity, the flow behavior did not seem to be considerably affected and difference of approximately 2 % was observed between FSI and CFD, for the maximum velocity magnitude. The change to a deformable artery promoted an increase in the maximum velocity observed but

a decrease in the average velocity, meaning that on average the artery deformation leads to a decrease in velocity, but in certain areas, namely in the bifurcation vicinity, this deformation leads to a higher local flow velocity.

Regarding wall shear stress, changing to a deformable artery promoted an increase in WSS with an increase of approximately 11.5 % in the maximum WSS observed. The average value of WSS also increased, but by only 2 %. An increase in the artery elasticity modulus also promoted a slight increase in the average WSS observed, but the maximum value was approximately maintained, with minor changes.

To conclude, an FSI model was successfully implemented, using a commercial software, to simulate the flow dynamics and structural behavior of an Iliac Bifurcation, representing an anatomical geometry in a more realistic method. This modeling methodology can be a useful tool to further analyze this type of arteries, but also other blood vessels or even other organs ia a more realistic way.

5 REFERENCES

[1] Carvalho V. Carneiro F, Ferreira A, Gama V, Teixeira, JC, Teixeira, S. Numerical study of the unsteady flow in simplified abd realistic iliac bifurcation models. Fluis 2021, 6, 284.

[2] Costa JMC, Fernandes FAO, Alves de Sousa RJ. Prediction of subdural haematoma based on a detailed numerical model of the cerebral bridging veins. J Mech Behav Biomed Mater 2020;111. https://doi.org/10.1016/j.jmbbm.2020.103976.

[3] Wesly RLR, Vaishnav RN, Fuchs et a. JCA, Patel DJ, Greenfield JC. Static linear and nonlinear elastic properties of normal and arterialized venous tissue in dog and man. Circ Res 1975;37:509–20. https://doi.org/10.1161/01.RES.37.4.509.

[4] Silver FH. In Vivo Non-Invasive Analysis of the Mechanical Properties of Vessel Walls using Vibrational Optical Coherence Tomography. Online J Cardiol Res Reports 2021;5:1–8. https://doi.org/10.33552/ojcrr.2021.05.000603.

[5] Camasão DB, Mantovani D. The mechanical characterization of blood vessels and their substitutes in the continuous quest for physiological-relevant performances. A critical review. Mater Today Bio 2021;10. https://doi.org/10.1016/j.mtbio.2021.100106.

[6] Hasan A, Memic A, Annabi N, Hossain M, Paul A, Dokmeci MR, et al. Electrospun scaffolds for tissue engineering of vascular grafts. Acta Biomater 2014;10:11–25. https://doi.org/10.1016/j.actbio.2013.08.022.

[7] Stekelenburg M, Rutten MCM, Snoeckx LHEH, Baaijens FPT. Dynamic straining combined with fibrin gel cell seeding improves strength of tissue-engineered small-diameter vascular grafts. Tissue Eng - Part A 2009;15:1081–9. https://doi.org/10.1089/ten.tea.2008.0183.

[8] Wuyts FL, Vanhuyse VJ, Langewouters GJ, Decraemer WF, Raman ER, Buyle S. Elastic properties of human aortas in relation to age and atherosclerosis: A structural model. Phys Med Biol 1995;40:1577–97. https://doi.org/10.1088/0031-9155/40/10/002.

[9] Monea AG, Baeck K, Verbeken E, Verpoest I, Sloten J Vander, Goffin J, et al. The biomechanical behaviour of the bridging vein-superior sagittal sinus complex with implications for the mechanopathology of acute subdural haematoma. J Mech Behav Biomed Mater 2014;32:155–65. https://doi.org/10.1016/j.jmbbm.2013.12.007.

[10] Bergel DH. The static elastic properties of the arterial wall. J Physiol 1961;156:445–57. https://doi.org/10.1113/jphysiol.1961.sp006686.

[11] Luo K, Jiang W, Yu C, Tian X, Zhou Z, Ding Y. Fluid-Solid Interaction Analysis on Iliac Bifurcation Artery: A Numerical Study. Int J Comput Methods 2019;16. https://doi.org/10.1142/S0219876218501128.

[12] Kotmakova AA, Gataulin YA, Yukhnev AD, Zaitsev DK. The abdominal aorta bifurcation with iliac arteries: The wall elasticity effect on the flow structure. St Petersbg State Polytech Univ J Phys Math 2020;13:68–76. https://doi.org/10.18721/JPM.13407.

[13] Patel S, Usmani AY, Muralidhar K. Effect of aorto-iliac bifurcation and iliac stenosis on flow dynamics in an abdominal aortic aneurysm. Fluid Dyn Res 2017;49. https://doi.org/10.1088/1873-7005/aa6a6b.

[14] Xenos M, Bluestein D. Biomechanical Aspects of Abdominal Aortic Aneurysm (AAA) and its Risk of Rupture: Fluid Structure Interaction (FSI) Studies. Stud Mechanobiol Tissue Eng Biomater 2011;7:181–220. https://doi.org/10.1007/8415_2011_72.

[15] Drewe CJ, Parker LP, Kelsey LJ, Norman PE, Powell JT, Doyle BJ. Haemodynamics and stresses in abdominal aortic aneurysms: A fluid-structure interaction study into the effect of proximal neck and iliac bifurcation angle. J Biomech 2017;60:150–6. https://doi.org/10.1016/j.jbiomech.2017.06.029.

[16] Moore, J.E. Jr., Maier, S., E., Ku, D. N. e Boesiger, P. (1994) Hemodynamics in the Abdominal Aorta: a Comparison of in vitro and in vivo Measurements. Journal of Applied Physiology, Vol. 76, pp. 1520-1527.

[17] Lee, D. and Chen, J.Y. (2003) Pulsatile Flow Fields in a Model of Abdominal Aorta with its Peripheral Branches. Biomedical Engineering Applications Basis Communications, Vol. 15, pp. 170-178.

[18] Carneiro, F.; Ribeiro, V.G.; Teixeira, J.C.; Teixeira, S.F.C.F. Numerical Study of the Velocity Profile Effect in the Atherosclerosis Development. In Proceedings of the 4th Engineering Conference "Engenharias'07—Innovation and Development", Covilhã, Portugal, 21–23 November 2007.